Adsorption (2011) 17: 189–199
DOI 10.1007/s10450-010-9308-0

Adsorption and diffusion of argon in disordered nanoporous carbons

Jeremy C. Palmer · Joshua D. Moore · John K. Brennan · Keith E. Gubbins

Received: 13 May 2010 / Accepted: 24 November 2010 / Published online: 11 December 2010

Abstract Application-specific optimization of disordered nanoporous carbons remains a formidable challenge due to the difficulty in accurately characterizing their microstructures with current empirical methods. Using molecular simulation techniques, we investigated the adsorptive and diffusive behavior of argon in three models of disordered nanoporous carbons. We found that the structural and morphological differences between these models gave rise to distinct phenomenological properties. The adsorptive behavior of argon in both the low and high pressure regimes was enhanced dramatically in the models with more crystalline microstructures. As for dynamic properties, we found that the adsorbent's structure and energetic topology significantly alters the rates of diffusion as well as the characteristics of the underlying diffusion mechanisms.

Keywords Anomalous diffusion · Single-file diffusion · Nanoporous carbons · Simulation · Adsorption · Molecular dynamics · Activated carbons

J.C. Palmer (✉) · J.D. Moore · K.E. Gubbins
Institute for Computational Science and Engineering and Department of Chemical and Biomolecular Engineering, North Carolina State University, Raleigh, NC 27695, USA
e-mail: jcpalmer@ncsu.edu

Present address:
J.D. Moore
US Army Research Laboratory, Weapons and Materials Research Directorate, Aberdeen Proving Ground, MD 21005, USA

J.K. Brennan
US Army Research Laboratory, Weapons and Materials Research Directorate, Aberdeen Proving Ground, MD 21005, USA

1 Introduction

Disordered nanoporous carbons (DNCs) are highly heterogeneous materials that are used widely in environmental- and energy-related applications, such as water purification and carbon dioxide sequestering (Radosz et al. 2008), and as materials for electrolyte and gas storage (Dash et al. 2006). In addition to their nanoscopic porous features and high specific surface areas, which often lead to superior performance in many separation and storage-based applications, industrial scale usage benefits from low production cost since DNCs are synthesized from abundant precursors, such as woods, coconut shells, coals (Bansal and Goyal 2005) and crystalline carbides (Yushin et al. 2006). While properties such as the pore size distribution (PSD) and specific surface area (SSA) may be modulated through selection of the precursor material and synthesis conditions, complete optimization of DNCs for specific applications remains a formidable challenge due to difficulty in fully characterizing their structural features and the inherently microscopic dependence of the phenomena that take place within their confining pores (e.g., adsorption, diffusion and chemical reaction). These challenges are compounded in many real-world applications where multiple phenomena occur in concert. In such circumstances, the optimization requirements may be dramatically different from materials that are designed to enhance a single phenomenon.

The adsorptive properties of DNCs have been studied extensively using experimental methods (Bansal and Goyal 2005). However, the diffusive behavior of fluids confined in these materials has received less attention. Specialized techniques, such as neutron spin echo (NSE) spectroscopy, quasi-elastic neutron scattering (QNES), and pulsed field gradient nuclear magnetic resonance methods (PFG NMR), can collectively probe the dynamic behavior of confined flu-

ids on time scales ranging from nanoseconds to seconds (Jobic 2002). These methods have been used to study diffusion in ordered porous materials, such as zeolites, where interpretation of the results can be augmented by prior knowledge of the material's crystallographic structure (e.g., Jobic et al. 2001; Jobic 2002; Jobic et al. 2002). DNCs pose additional challenges due to their disordered microstructure and highly tortuous and interconnected porous features. Dubinin et al. (1988) used PFG NMR to measure diffusion coefficients for water, methanol and benzene in several activated carbons and found that their diffusivities were generally an order of magnitude or more lower than in the bulk liquid. The diffusivities of the three adsorbates were also found to decrease with the estimated pore size of the carbon by roughly the same factor, indicating that the decrease was predominately caused by differences in the tortuosity of the samples. Heink et al. (1993) later extended the work to mixtures of water and perfluorobenzene and discovered a similar dependence of the diffusivities on the average pore size. These conclusions, while well-justified by the available data, are somewhat dependent on the ability to accurately characterize the structures of the DNCs used in these studies. For example, it has been well established that estimated pore sizes are dependent on the methods chosen to perform the analysis (Lastoskie et al. 1993; Neimark et al. 2009). In many cases the accuracies of the characterization methods are simply not known. In addition, the limited availability of the equipment necessary to perform experimental diffusion studies is also problematic. The characteristics of the observed dynamics can be dependent on the resolution of the timescale available with the technique and particular instrument. Thus multiple methods and instruments may be required to probe all of the timescales of interest (Jobic et al. 2001). Moreover, the dynamic behavior observed with these methods is a spatial average over the entire material sample. Many materials, such as DNCs, have a variety of structural features that may give rise to different local modes of diffusion (Liu et al. 2010). A more fundamental understanding of this relationship could be the key to developing synthesis strategies for DNCs with tunable diffusive characteristics.

Atomistic simulation methods are ideally suited for complementing experimental studies of adsorptive and diffusive properties of confined nanoscale systems. They provide statistically-exact solutions for model systems, accessing timescales ranging from femto- to microseconds, while retaining atomic-level resolution and information concerning the behavior of individual atoms or molecules (Gubbins and Moore 2010). In many cases, the accessible range of time and length scales of these methods is sufficient such that the calculated quantities can be directly compared with empirical measurements. For these reasons, such approaches have been widely applied to study adsorption (Cracknell et al. 1993; Do and Do 2004; Cruz and Müller 2009a), diffusion (Cruz and Müller 2009b; Liu et al. 2010) and even chemical reactions (Turner et al. 2001; Santiso et al. 2005; Lísal et al. 2006) in idealized models of nanoporous carbons that consist of regularly-shaped, isolated pores. The challenge in extending these methods to study confinement effects in DNCs has been the lack of realistic structural models for these materials with features such as variable pore sizes and morphologies, chemical and structural surface heterogeneities and pore-pore connectivity. Several algorithms have been proposed to construct models that capture these features by generating DNC structures from more elementary building blocks such as aromatic rings and graphene fragments of various sizes and shapes (Biggs and Buts 2006; Herrera et al. 2009). These methods have achieved some success in describing the amorphous features of DNCs, however their predictive abilities are limited due to the fact that they do not address the heterogeneous nature of the local carbon chemistry using a more fundamental approach. Details of these and other methods have been the subject of reviews (Bandosz et al. 2003; Biggs and Buts 2006). Recent progress has been made in developing statistical mechanics based methods using both *reconstructive* approaches (Jain et al. 2006; Opletal et al. 2002; Palmer et al. 2009) that produce models with the aid of experimental measurements, and *mimetic* approaches (Shi 2008; Palmer et al. 2010) that generate models by mimicking aspects of the experimental synthesis processes. Both approaches use reactive intermolecular force fields (e.g., Brenner 1990; Marks 2000; van Duin et al. 2001) to describe the formation and destruction of carbon-carbon bonds from physical principles. Models developed with these methods have been shown to predict qualitatively (Palmer et al. 2010), and in some cases quantitatively (Palmer et al. 2009), experimental quantities related to the structural and energetic topology of the target materials, including adsorption isotherms and enthalpies of adsorption.

In this study, we investigate the adsorptive and diffusive behavior of argon in three nanoporous carbon models developed in previous work (Palmer et al. 2010) that utilized the quench molecular dynamics (QMD) method of Shi (2008). In the QMD approach, the structures are generated by thermally quenching a gas-phase carbon into an amorphous solid-phase carbon. By controlling the quenching rate, properties such as the local carbon bonding structures, PSDs and SSAs may be finely tuned. While this approach is not strictly mimetic, the variations in structural properties that arise by changing the quench rate have been shown to be qualitatively similar to those observed in experimental systems as the synthesis temperature is appropriately adjusted (Palmer et al. 2010). Moreover, the QMD method is highly predictive in that the final structural model is only dependent on intensive properties, namely the average carbon density and thermal quench rate. The three

QMD-generated models examined in this study have different microtextures and porous features, but identical average carbon densities. Therefore, the impact that these morphological differences have on adsorptive and diffusive behavior on argon can be studied over a range of state conditions. In particular, the effects of changes in the structural ordering, distribution of pore sizes, and accessible volumes are investigated. We demonstrate that these differences give rise to distinct adsorptive properties, showing a large increase in their total capacity of argon as the structures become more highly ordered. Finally, we also show that diffusion in the different models not only occurs at different rates but also by different mechanisms, and that the pore size distribution alone is an insufficient indicator of the diffusive properties of DNCs.

2 Computational methods

2.1 Carbon model generation

The three model DNCs examined in this study were generated using the QMD method of Shi (2008). A brief overview of the procedure is given below, with full details found elsewhere (Palmer et al. 2010). The same initial and final temperatures were used to generate each of the three models, while the quench rate was systematically varied to produce structures with different morphologies. The slowest quench rate, 2.5×10^{12} K/s, was selected to generate a highly ordered structure consisting of large planar graphene fragments. The other two models were generated using quench rates 8 and 64 times faster than the slowest quench rate, which resulted in more amorphous structures. The simulations were carried out in periodic, cubic unit cells ranging from ~4.15–4.37 nm in length. After the quenching process, any singlet carbon atoms were removed from the structures. The initial carbon densities at each quench rate were chosen to produce final structures with average densities of 0.94 g/cm^3, corresponding to ~3,300–3,900 carbon atoms in the unit cells.

2.2 Grand canonical Monte Carlo simulations

Adsorption isotherms for argon were determined for the three model carbon structures using the grand canonical Monte Carlo (GCMC) method (Norman and Filinov 1969), which is used to simulate an open system in equilibrium with an infinite reservoir containing the bulk fluid phase at the same temperature and chemical potential. The number of molecules in the adsorbed phase is allowed to fluctuate until chemical equilibrium is reached with the reservoir. In practice, only the chemical potential and temperature are specified and the bulk phase is not simulated explicitly. If the bulk phase is assumed to be an ideal gas at the state conditions considered, then the imposed chemical potential can be related to the bulk pressure using the ideal gas equation of state. If the assumption of ideality does not hold, the relationship between the chemical potential and pressure may be obtained using a more appropriate equation of state or by performing additional simulations in the isobaric-isothermal (NPT) ensemble (Wood 1968) while using a suitable method to calculate the chemical potential (Frenkel and Smit 2002 and references therein).

In this study, argon was modeled as a single site Lennard-Jones (LJ) molecule with $\sigma_{Ar} = 0.3405$ nm and $\varepsilon_{Ar}/k_B = 119.8$ K. The carbon structures were modeled as rigid, with each carbon atom having effective LJ parameters of $\sigma_C = 0.34$ nm and $\varepsilon_C/k_B = 28.0$ K as prescribed by Steele (1973). Lennard-Jones parameters for the carbon-fluid interactions were estimated using the Lorentz-Berthelot combining rules (i.e., $\sigma_{ij} = (\sigma_{ii} + \sigma_{jj})/2$ and $\varepsilon_{ij} = \sqrt{\varepsilon_{ii}\varepsilon_{jj}}$). All interatomic pair interactions were truncated at $5\sigma_{ij}$ (with no long-range corrections added) and distances were calculated according to the minimum image convention (Allen and Tildesley 1989).

Isotherms were simulated for argon at 87.3 and 120 K at chemical potentials corresponding to reduced pressures ranging from $P/P_\circ \sim 10^{-8}$–1, where $P_\circ$ is the bulk saturation pressure. To obtain an appropriate relationship between the chemical potential and bulk pressure for argon, the LJ equation of state of Johnson et al. (1993) was used. The GCMC simulations were run for a total of 10^8 MC moves at each chemical potential, with statistics collected over the second half of the simulations. To expedite equilibration, final configurations of fluid molecules were used as starting configurations for the simulations performed at subsequent chemical potentials along the adsorption isotherms. In addition to adsorption isotherms, isosteric heats of adsorption, q_{st}, were also calculated from the GCMC simulations using the fluctuation method (Nicholson and Parsonage 1982; Vuong and Monson 1996),

$$q_{st} = RT - \frac{\langle UN\rangle - \langle U\rangle\langle N\rangle}{\langle N^2\rangle - \langle N\rangle^2} \tag{1}$$

where U is the configurational energy, N is the number of molecules, R is the gas constant and the brackets indicate that the quantities are ensemble averages.

2.3 Molecular dynamics simulations

The dynamical behavior of argon confined within the DNCs was examined using molecular dynamics (MD) simulations (Alder and Wainwright 1957) with the LAMMPS (Large-scale Atomic/Molecular Massively Parallel Simulator) software package (Plimpton 1995). Each MD simulation was

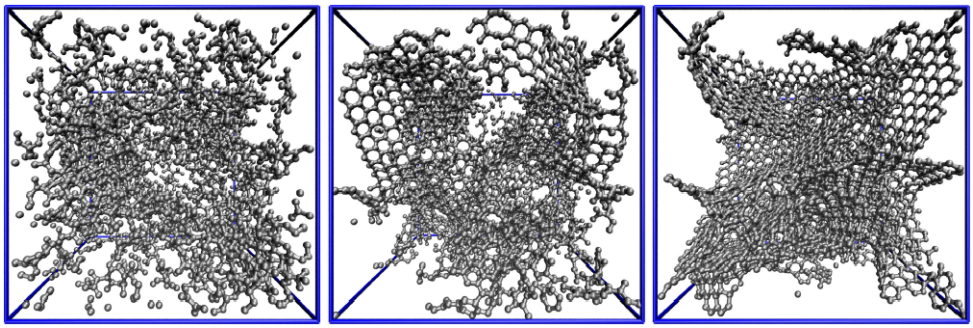

Fig. 1 Snapshots of three nanoporous carbon structures obtained from quench molecular dynamics simulations at relative quench rates of 64 (*left*), 8 (*center*) and 1 (*right*). *Grey beads and cylinders* represent center of mass positions of carbon atoms and C-C bonds, respectively

initiated from an equilibrated configuration of adsorbed argon atoms obtained from the GCMC simulations. In order to ensure that adequate statistics could be obtained even under low loading conditions, supercells containing a minimum of 500 argon atoms were constructed by replicating the GCMC configurations across the periodic boundaries of the unit cell. The initial velocities of the argon atoms in the supercells were sampled from a Maxwell-Boltzmann distribution at the desired temperature. The systems were first equilibrated in the canonical (NVT) ensemble for 1 ns, in which the Nosé-Hoover thermostat (Nosé 1984; Hoover 1985) with a 0.001 ps damping constant was used, followed by a production phase of 10 ns in the microcanonical (NVE) ensemble. In both the NVT and NVE simulations, a timestep of 1 fs was used to integrate the equations of motion, and interatomic interactions were smoothed to zero between distances of 4.9σ and 5.5σ to ensure continuity of the LJ potential and force. During the microcanonical production phase, the mean-square displacement (MSD) of argon molecules was calculated using multiple time origins every 25 ps and the temperature was monitored to ensure that fluctuations did not exceed ± 5 K about the desired temperature.

3 Results and discussion

3.1 Structural and morphological features

The three model carbon structures, denoted as Q64, Q8 and Q1 in the subsequent discussion to indicate the relative quench rate at which they were generated, had very different morphological features, increasing in structural order as the relative quench rate was decreased from 64 to 1. As illustrated in Fig. 1, the model generated at the fastest quench rate (Q64), consisted of small carbon fragments containing only a few carbon atoms. As the relative quench rate was decreased to 8, the carbon atoms had sufficient time to aggregate and form larger carbon fragments. At the slowest quench rate (Q1), the final carbon structure consisted entirely of intertwined graphene sheets, each containing hundreds of carbon atoms.

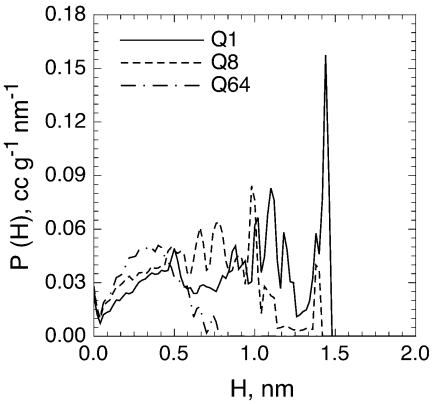

Fig. 2 Total geometric pore size distributions calculated using the method of Gelb and Gubbins (1999) for the simulated nanoporous carbons

The increased size of the carbon fragments had a substantial impact on both the pore size distribution and pore structure. Using the method of Gelb and Gubbins (1998), the total pore size distribution (PSD) for each of the three model carbons was calculated. In their method, the pore size at a given point in the structure is determined by finding the diameter of the largest sphere that encompasses the point without overlapping with the pore walls. The unit cells containing the structures were mapped onto a grid with 0.02 nm spacing between points. The pore sizes were calculated at each of the grid points and then compiled into a histogram that was then differentiated and normalized to obtain the PSD, or $P(H)$, where H is the pore width. As evident from Fig. 2, the PSD broadened by nearly a factor of two as the quench rate was decreased. The larger, more planar graphene fragments that formed at slower quench rates created more open porous structures, while the smaller graphene fragments found at faster quench rates formed branch-like structures that frequently bisected the void space, creating smaller pores. Even though significantly larger pores emerged at slower quench rates, the geometric volume of small pores did not decrease dramatically, indicating that the total void volume increased.

While changes in the geometric volumes unoccupied by the carbon network are indicative of morphological differences in the carbon structures, the accessible pore volumes

Table 1 Summary of structural properties of the model carbons

Relative quench rate	Accessible volume, V_{acc} (cm^3/g)	True density, ρ_C^{true} (g/cm^3)	Geometric SSA, S_{geo} (m^2/g)	BET SSA, S_{BET} (m^2/g)
64	0.23	1.20	769	674
8	0.46	1.67	1547	1188
1	0.53	1.89	1470	1473

are more important quantities in examining the thermodynamic state of confined fluids (Gelb and Gubbins 1998). Following the prescription of Myers and Monson (2002), the accessible volumes of the porous structures were estimated using Monte Carlo integration with helium ($\sigma_{He} = 0.2557$ nm, $\varepsilon_{He}/k_B = 10.22$ K) (Tchouar et al. 2003) as a probe molecule at 298 K. The results of these calculations, presented in Table 1, showed more than a two-fold increase in the accessible volume as the quench rate was decreased. Since the average carbon density was the same for each of the models, the increase in accessible volume suggested an increase in the local carbon density due to a more crystalline-like bonding structure. These results were qualitatively consistent with the simulation snapshots shown in Fig. 1. The local crystalline density, or true density, is measured experimentally using helium pycnometry (Tsai and Chang 1994) and is defined as the mean density of the sample divided by the void fraction that is inaccessible to helium gas: $\rho_C^{true} = \bar{\rho}_C/(1 - V_{acc}/V_{total})$. From the accessible volumes, the densities for the three models were calculated and are summarized in Table 1. The appropriate crystalline reference under the state conditions used to generate the models is graphite, which has a true density of approximately 2.23 g/cm^3 (Wyckoff 1963). Thus it was apparent from these values that the structures also became more crystalline in their density as the quench rate was decreased.

Specific surface areas (SSAs) of the carbon structures were also calculated from the geometry of the models. Experimentally, SSAs are almost always estimated from adsorption isotherms of nitrogen at 77.4 K or argon at 87.3 K by fitting to simple theoretical models such as the BET or Langmuir isotherm equations. The procedure estimates the number of molecules that must adsorb to form a complete monolayer on the surface of the porous material (Gregg and Sing 1967). The SSA may then be obtained by multiplying the effective cross-sectional area of a single molecule by the number of molecules in the monolayer. Unfortunately, the models that are most often used, such as the BET equation, make assumptions concerning the adsorption mechanism and energetic topology of the surface that may not be valid in highly heterogeneous, confined materials (Rouquerol et al. 2007).

An alternative approach for model systems is to use an unambiguous definition of the SSA based on structural or energetic criteria. A geometric estimate of the SSA that corresponds to the surface accessible to the center of a probe molecule as it "rolls" along the surface of the structure was calculated using the Monte Carlo integration method described by Thomson and Gubbins (2000) with an argon-sized probe molecule. For comparison, the BET surface area was also calculated from the simulated argon isotherms at 87.3 K. The pressure range used for the BET calculations was determined using the procedure described by Rouquerol et al. (2007). The results of both methods are shown in Table 1. The geometric SSA estimates showed that the surface area was smallest for the most disordered structure (Q64) due to the formation of small, inaccessible pores. As the structures became more ordered (Q8), the SSA increased dramatically due to the formation of larger, accessible pores. However, for the most ordered structure (Q1), the surface area decreased compared to Q8 because of the presence of larger graphene fragments that had less accessible surface area. In addition to under predicting the surface areas of the two most disordered structures, the BET estimates erroneously predicted that the surface areas should monotonically increase with the structural ordering. Presently, explanations for the discrepancies between the geometric and BET SSA estimates are not entirely clear. Interestingly, near perfect agreement was found for the most ordered structure, Q1, which contained the largest pores and the most regularly-shaped carbon fragments.

3.2 Adsorptive behavior

To assess the role of morphology of the model structures on the adsorptive properties, adsorption isotherms for argon were simulated at 87.3 K and 120 K, where Fig. 3 shows the isotherms for all three models. All of the isotherms were Type I reversible isotherms characteristic of microporous solids (Gregg and Sing 1967), with no observable hysteresis upon desorption. For clarity, the desorption branches of the isotherms have been omitted from Fig. 3. The primary difference between the isotherms at 87.3 K and 120 K was that the pore filling region was shifted to higher pressures at 120 K due to the increased thermal energy of the adsorbing molecules, which made adsorption less favorable at the same bulk pressures.

The most noticeable feature in comparing the isotherms for the three structures at the same temperatures was the

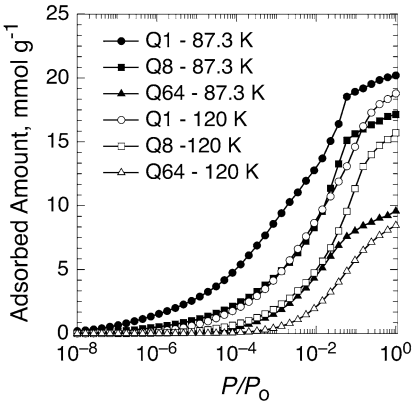

Fig. 3 Adsorption isotherms of argon at 87.3 K (*closed symbols*) and 120 K (*open symbols*) for the three nanoporous carbon structures

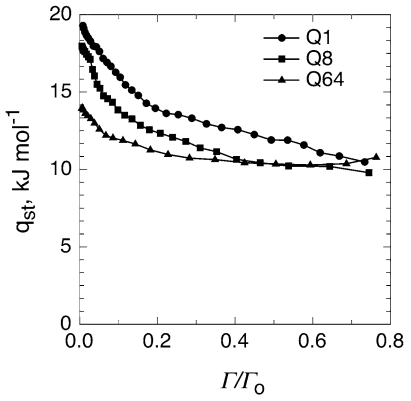

Fig. 4 Isosteric heats as a function of the reduced loading ($\Gamma/\Gamma_\circ$) for argon at 87.3 K in the three nanoporous carbon structures

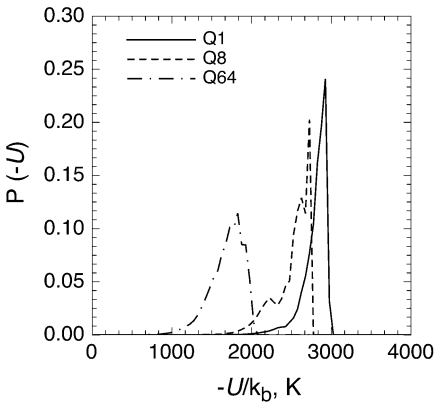

Fig. 5 Zero-coverage solid-fluid potential energy distributions for argon at 87.3 K on the three nanoporous carbon models

difference in the amount of argon adsorbed near the bulk saturation pressures. Since the porous framework enhances adsorption, it was expected that at pressures somewhat lower than the bulk saturation pressure the adsorbed fluid would reach liquid-like densities if changes in the packing structure due to the confinement could be neglected. To confirm this, the liquid density of argon at the saturation pressure, ρ_{Ar}^{liquid} (87.3 K; 1 bar) = 34.931 mmol/cm^3 (Lemmon et al. 2010), was used to estimate the accessible pore volume from the total amount of argon adsorbed at $P/P_\circ = 1$. Such a procedure is often used experimentally to estimate the pore volumes from adsorption data (Gregg and Sing 1967). The estimated volumes at 87.3 K were 0.27, 0.49 and 0.58 g/cm^3, for the Q64, Q8 and Q1 structures, respectively. These results are in reasonable agreement with the earlier estimates obtained using helium, shown in Table 1. The discrepancies, ~16%, 7% and 9%, respectively, were less for the more ordered structures, Q8 and Q1, indicating that significant differences in the adsorbed fluid structure from that of the bulk liquid state occurred due to the presence of small pores in the Q64 structure.

In addition to the larger adsorption capacities observed in the more ordered models, an increase in the amount adsorbed at low relative pressures also occurred. Rationalizing by considering the pore size distributions alone, it was expected that the Q64 and Q8 structures would adsorb more argon in the low pressure regime due to their higher fraction of smaller pores, which would provide more energetically favorable sites for adsorption. This apparent inconsistency was resolved by calculating the isosteric heats of adsorption for argon at 87.3 K using (1). Isosteric heats provide detailed information concerning the energetics of adsorption along the isotherm. Under low loading/low pressure conditions, when there are only a few fluid molecules adsorbed, the behavior of q_{st} is dictated by the interactions between the adsorbing fluid and porous structure. Thus it can provide information concerning both the microtexture of the solid and the low-pressure adsorption mechanisms. At higher loadings and pressures, the isosteric heat is dominated by fluid-fluid interactions and provides information concerning the nature of the confined fluid. As shown in Fig. 4, the values of q_{st} in the low loading regime became significantly larger as the order of the structures increased despite the presence of larger pores. This trend, along with the adsorption isotherm trends, indicated that stronger effective fluid-solid interactions resulted in increased adsorption in the low pressure regions of the isotherms. The increase in the fluid-solid interactions was likely a result of the higher local density of carbon of the confining surfaces due to the more crystalline nature of the graphene fragments in the models produced at slower quench rates.

Boltzmann-weighted energy distributions, $P(U) = \int \delta(U - U(\mathbf{r})) \exp(-U(\mathbf{r})/RT)\, dV/Q$, were also constructed for argon at 87.3 K, with a normalization constant, $Q = \int \exp(-U(\mathbf{r})/RT)\, dV$, where $U(\mathbf{r})$ is the fluid-solid potential of an argon molecule placed at position $\mathbf{r}$ in the simulation cell. The histograms were calculated in a manner similar to the accessible volume, with the appropriate exponential weights applied to the energy at each sampled point. The resulting distributions, shown in Fig. 5, illustrate the

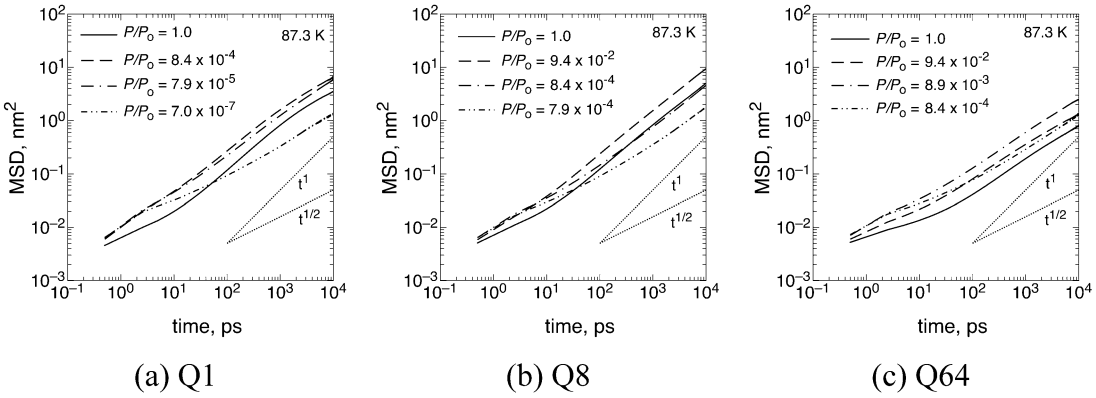

Fig. 6 Mean-square displacement of argon in the three nanoporous carbons at 87.3 K: (**a**) Q1, (**b**) Q8, (**c**) Q64. Reference lines (*dotted*) illustrating t^1 and $t^{1/2}$ dependence are also shown

extent of energetic heterogeneity of each of the structures. The histograms for the more ordered structures, Q8 and Q1, had very little overlap with the histogram of Q64. This explained the low loading adsorption behavior of the isotherms by demonstrating that the ordered structures contained adsorption sites that were much more energetically favorable under the state conditions examined. The width of the histograms also decreased with the quench rate. This showed that along with the increased carbon density of the confining surfaces, the energetic topology becomes more regular as the structures became more crystalline.

3.3 Dynamic behavior

The morphological differences of the carbon models clearly had an impact on the adsorptive behavior of argon, significantly affecting both the total adsorption capacity and the energetics of adsorption. The influence of structural features on the dynamic behavior of confined argon is likewise of interest, since the efficiency of many separations and energy storage applications that utilize DNCs are limited by slow diffusion rates of molecules in and out of the nanopores.

To examine the dynamic behavior of the confined argon, we used molecular dynamic simulations. From the resulting trajectories, mean-square displacements (MSDs) were calculated. For systems of molecules undergoing a random walk in three dimensions, or Fickian diffusion, the long-time behavior of the MSD is proportional to time: $\lim_{t\to\infty}\langle[\mathbf{r}(t)-\mathbf{r}(t_0)]^2\rangle = 6Dt$, where $\mathbf{r}$ is the molecule's position, t is the time elapsed relative to an arbitrary reference time, $t_\circ$, and D is a constant of proportionality known as the self-diffusion coefficient. Other types of behavior can also be observed in highly confined systems, where constraints are imposed on the motions of the molecules. In such cases, the MSD can be proportional to t^n, where $n \in [1/2, 1)$. Diffusion mechanisms with these types of phenomenological characteristics are collectively known as sub-diffusive or anomalous diffusion modes (Gubbins et al. 2011; Hahn and Kärger 1998; Moore et al. 2010), and they are much slower than Fickian diffusion. In the limiting case where molecules are restricted to a one-dimensional random walk (Felderhof 2009), such as diffusion in small corrugated carbon nanotubes (Hahn and Kärger 1996), molecules are unable to pass each other and single-file diffusion occurs. For single-file diffusion, the MSD exhibits a characteristic $t^{1/2}$ dependence.

Representative examples of MSDs calculated at different pressures along the isotherms at 87.3 K and 120 K are shown in Figs. 6 and 7, respectively. On a log-log scale, the slope of the MSD is indicative of its dependence on time, while the intercept of the linear region of the MSD is directly related to the self-diffusion coefficient. At 87.3 K, all of the MSDs for argon showed a nearly $t^{1/2}$ dependence at short times (∼10–50 ps), which indicated that argon frequently collided with the pore walls due to a high degree of confinement. At longer times (>100 ps), the slope of the MSDs increased as a result of the molecules escaping from their highly attractive adsorption sites into less confined regions. This interpretation was confirmed by visual examination of the MD trajectories. At 120 K, the duration of the slower modes was reduced due to the increased kinetic energy of the molecules, which allowed them to escape the local potential minima of the adsorption sites at a faster rate than at 87.3 K.

For timescales on the order of nanoseconds, the slope of the MSDs approached unity for the Q8 model at both 87.3 K and 120 K, indicating the behavior of the confined argon molecules, on average, satisfied the three-dimensional random walk criterion for Fickian diffusion (*i.e.*, the behavior had become diffuse). However, even at 10 ns, strictly Fickian behavior was not observed in either the Q64 or Q1 models. These results appeared to contradict experimental observations (Dubinin et al. 1988; Heink et al. 1993) that showed a monotonic increase in the diffusion coefficient

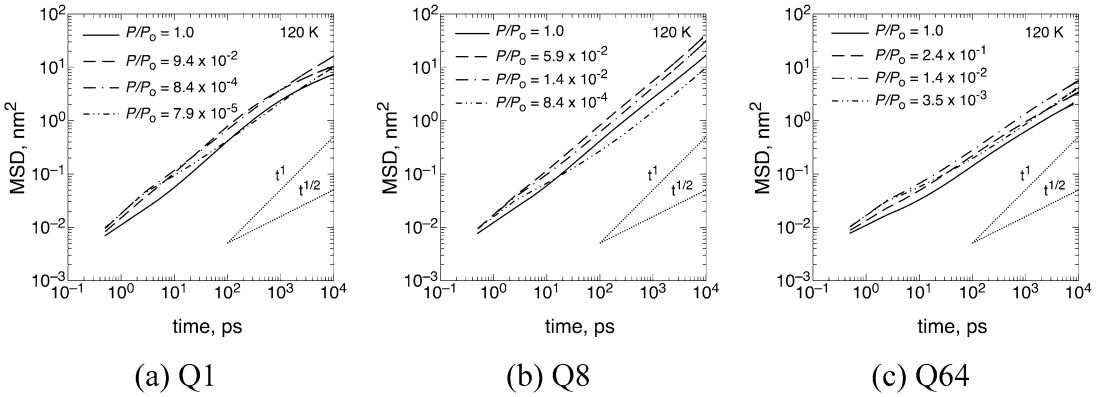

Fig. 7 Mean-square displacement of argon in the three nanoporous carbons at 120 K: (**a**) Q1, (**b**) Q8, (**c**) Q64. Reference lines (*dotted*) illustrating t^1 and $t^{1/2}$ dependence are also shown

with pore size. Since the Q64 model contained exclusively sub-nanometer pores, it was not unexpected that anomalous diffusive behavior would be observed. Liu et al. (2009) have recently shown that in carbon nanotubes, the crossover from anomalous to Fickian diffusion occurs when the accessible pore size of the nanotube, $H_{acc} = H - \sigma_{Ar-C}$, is ∼1.76 molecular diameters wide. This corresponds to a geometric pore size of $\sim 2.76\sigma_{Ar}$ (∼0.94 nm), which is larger than the maximum pore size observed in the PSD for Q64. Both the Q8 and Q1 structures had pores that were appreciably larger than this cutoff, but only the argon confined within the Q8 structure exhibited Fickian behavior.

The magnitudes of the mean-square displacements of argon were observed with a maximum at an intermediate pressure in each of the structures at 87.3 K and 120 K. At 87.3 K (Fig. 6), these maxima occurred near $P/P_\circ \sim 8.4 \times 10^{-4}$, 9.4×10^{-2}, and 8.9×10^{-2} in the Q1, Q8 and Q64 structures, respectively. At 120 K (Fig. 7), they were observed near $P/P_\circ \sim 9.4 \times 10^{-2}$, 5.9×10^{-2}, and 1.4×10^{-2} in the Q1, Q8 and Q64 structures, respectively. These relative pressures are in the pore filling region of the isotherms in Fig. 3. In materials with regularly shaped pores (such as carbon nanotubes), the mean-square displacement is expected to decrease with increasing pressure (Liu et al. 2009) as an increased density of fluid generally slows diffusion. In the DNCs the diffusion of argon is slow at low relative pressure due to fluid molecules being strongly adsorbed in the pores. At intermediate pressure, when the smallest pores are completely filled, the larger pores begin to fill and the overall rate of diffusion increases due to the faster movement of atoms in the larger pores. However, analogous to the behavior observed in regularly shaped pores, the rate of diffusion decreases at higher pressures. This leads to an observed maximum in the mean-square displacement at intermediate pressures.

Since a maximum in the mean-square displacement was observed, we also would expect a maximum to occur for the self-diffusion coefficient as a function of pressure. However, we do not report estimates or comparisons of the self-diffusivities of argon in the three structures due to the fact that completely diffusive (Fickian) behavior was not observed for argon diffusing in Q1 and Q64 within the limits of our simulations (10 ns). Longer simulations (> 100 ns) would be needed to observe completely diffusive (Fickian) behavior of argon in Q1 and Q64, and we predict that maxima in the self-diffusion coefficients would be observed for all three structures at longer times. We previously observed a maximum in the diffusion coefficient for argon diffusing in both BPL activated carbon and a carbon replicate of Faujasite (Moore et al. 2010) where the diffusive regime was reached. This behavior has also been observed in both simulations of several LJ fluids in saccharose-derived carbons (Pikunic and Gubbins 2003; Coasne et al. 2006; Nguyen et al. 2006; Coasne et al. 2007), as well as experimentally for molecular fluids in zeolites (Brandani et al. 1995) and water in activated carbon (Kärger et al. 1989).

Mean-square displacements were also calculated at 300 K, 500 K and 1000 K (Fig. 8) using initial configurations from the isotherms at 87.3 K that corresponded to loadings of approximately 70% of the total adsorption capacity for each structure. These configurations roughly corresponded to relative pressures at which: (i) the smallest pores were filled; and (ii) pore filling started to occur for the isotherms shown in Fig. 3. At the higher temperatures, the diffusive behavior in Q8 remained unchanged; however, at the longest times (close to 10 ns) the slope of the MSDs in Q1 also tended towards unity, indicating that the diffusive (Fickian) regime was close to being reached. The difference between the MSDs at 87.3 K and the higher temperatures for Q1 was not attributed to the extent of confinement resulting from the presence of small pores, as was the case for the Q64 structure, but rather to the strength of the interactions between the adsorbed argon molecules and the pore walls. As illustrated in Fig. 5, the fluid-solid interactions are about

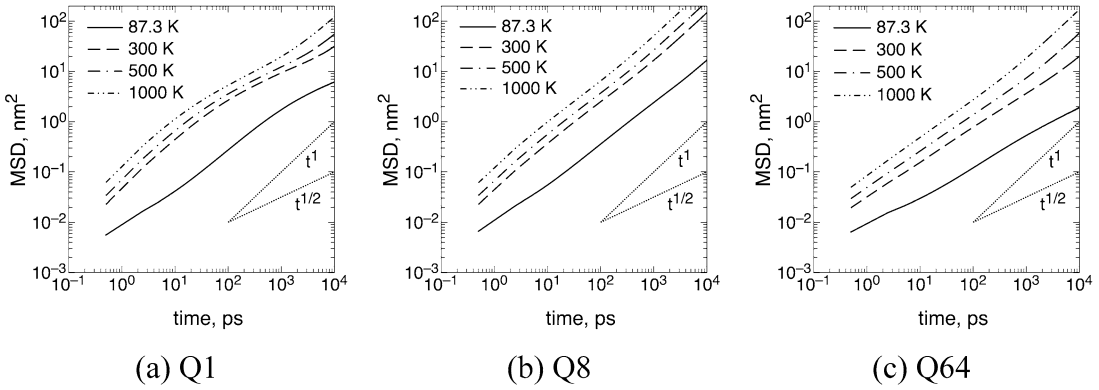

Fig. 8 Mean-square displacement of argon in the three nanoporous carbons at 87, 300, 500, and 1000 K at approximately 70% loading: (**a**) Q1, (**b**) Q8, (**c**) Q64. Reference lines (*dotted*) illustrating t^1 and $t^{1/2}$ dependence are also shown

$\sim 5k_BT$ larger on average for the Q1 structure than for the Q8 structure due to the increased crystallinity of the pore walls. The stronger affinity of the pore walls caused the molecules to reside for longer time periods at their highly confined adsorption sites. At increased temperatures the adsorbed molecules could more readily escape from their adsorption sites, reducing the effective extent of confinement and shifting the observed mechanism from anomalous to Fickian. Thus, while the diffusion of argon in the Q64 structure was anomalous due to steric hindrances, the Q1 model imposed energetic limitations on the diffusive motions.

4 Conclusions

Accurate characterization and optimization of microporous materials, in particular materials with disordered microstructures, remains a major hurdle in the development of more efficient separation processes and energy storage devices. Using molecular simulation methods, we have gained insight into the role that the structural morphology of DNCs plays in determining the adsorptive and diffusive behaviors of argon. We have demonstrated that both the total adsorption capacity and low pressure adsorption behavior can be dramatically altered by changes in the local bonding structure of DNCs. In general, we found that models with more crystalline-like microstructures exhibited larger adsorption capacities as a result of having greater accessible pore volumes. The larger pore-wall density in the more ordered structures also had a significant enhancement on the adsorption in the low pressure regimes due to stronger effective fluid-wall interactions. However, this feature seemed to have a detrimental impact on the dynamic behavior, causing the confined fluid to take on a slow, sub-diffusive mode of transport, despite the presence of large pores in the material. Similar behaviors were only observed in structures with much smaller characteristic pore sizes. These findings contradict experimental studies that have shown a monotonic increase in the diffusion rate as the pore size is increased. In order to completely understand this discrepancy as well as the overall diffusive behavior in these materials, longer time scales must be considered. Albeit the MD trajectories in this study were long in comparison with other studies, they were too short to observe the complete transition from anomalous to Fickian behavior in all of the cases and thus proper estimates of the self-diffusivities could not be obtained. From these preliminary findings, we have estimated that trajectories in excess of 100 ns (10× our current trajectories) may be necessary to observe such transitions at moderate temperatures. The computational cost of the simulations for such long durations is a major drawback and is the likely reason that examining long-time diffusion behavior with atomistic MD methods is not more commonplace.

Acknowledgements J.C.P. gratefully acknowledges support from the US Defense Threat Reduction Agency (Project ID: AA07CBT011). J.D.M. benefited from support from the U.S. National Science Foundation (grant number CBET-0932656). Computational time was provided through a Teragrid Research Allocation by the U.S. National Science Foundation (grant No. CHE080046N).

References

Alder, B.J., Wainwright, T.E.: Phase transitions for hard spheres. J. Chem. Phys. **27**, 1208–1209 (1957)

Allen, M., Tildesley, D.: Computer Simulation of Liquids. Oxford University Press, Oxford (1989)

Bandosz, T., Biggs, M., Gubbins, K.E., Hattori, Y., Iiyama, T., Kaneko, K., Pikunic, J., Thomson, K.: Molecular models of porous carbons. In: Radovic, L. (ed.) Chemistry and Physics of Carbon, vol. 28, pp. 41–228. Marcel Dekker, New York (2003)

Bansal, R., Goyal, M.: Activated Carbon Adsorption. CRC Press, Boca Raton (2005)

Biggs, M., Buts, A.: Virtual porous carbons: what they are and what they can be used for. Mol. Simul. **32**, 579–593 (2006)

Brandani, S., Ruthven, D.M., Karger, J.: Concentration-dependence of self-diffusivity of methanol in NaX zeolite crystals. Zeolites **15**, 494–495 (1995)

Brenner, D.: Empirical potential for hydrocarbons for use in simulating the chemical vapor deposition of diamond films. Phys. Rev. B: Condens. Matter Mat. Phys. **42**, 9458–9471 (1990)

Coasne, B., Jain, S.K., Gubbins, K.E.: Adsorption, structure and dynamics of fluids in ordered and disordered models of porous carbons. Mol. Phys. **104**, 3491–3499 (2006)

Coasne, B., Jain, S.K., Gubbins, K.E.: Adsorption and dynamics of argon in porous carbons. Eur. Phys. J. Spec. Top. **141**, 121–125 (2007)

Cracknell, R., Nicholson, D., Quirke, N.: A grand canonical Monte Carlo study of Lennard-Jones mixtures in slit shaped pores. Mol. Phys. **80**, 885–897 (1993)

Cruz, F., Müller, E.: Behavior of ethylene and ethane within single-walled carbon nanotubes. 1. Adsorption and equilibrium properties. Adsorption **15**, 1–12 (2009a)

Cruz, F., Müller, E.: Behavior of ethylene and ethane within single-walled carbon nanotubes, 2. Dynamical properties. Adsorption **15**, 13–22 (2009b)

Dash, R., Chmiola, J., Yushin, G., Gogotsi, Y., Laudisio, G., Singer, J., Fischer, J., Kucheyev, S.: Titanium carbide derived nanoporous carbon for energy-related applications. Carbon **44**, 2489–2497 (2006)

Do, D., Do, H.: Effects of potential models on the adsorption of ethane and ethylene on graphitized thermal carbon black. Study of two-dimensional critical temperature and isosteric heat versus loading. Langmuir **20**, 10889–10899 (2004)

Dubinin, M.M., Vartapetian, R.S., Voloshchuk, A.M., Kärger, J., Pfeifer, H.: NMR study of translational mobility of molecules adsorbed on active carbons. Carbon **26**, 515–520 (1988)

Felderhof, B.U.: Fluctuation theory of single-file diffusion. J. Chem. Phys. **131**, 064504 (2009)

Frenkel, D., Smit, B.: Understanding Molecular Simulation: From Algorithms to Applications. Academic Press, San Diego (2002)

Gelb, L.D., Gubbins, K.E.: Characterization of porous glasses: simulation models, adsorption isotherms, and the Brunauer-Emmett-Teller analysis method. Langmuir **14**, 2097–2111 (1998)

Gelb, L., Gubbins, K.E.: Pore size distributions in porous glasses: a computer simulation study. Langmuir **15**, 305–308 (1999)

Gregg, S.J., Sing, K.S.W.: Adsorption, Surface Area, and Porosity. Academic Press, London (1967)

Gubbins, K.E., Moore, J.D.: Molecular modeling of matter: impact and prospects in engineering. Ind. Eng. Chem. Res. **49**, 3026–3046 (2010)

Gubbins, K.E., Liu, Y.-C., Moore, J.D., Palmer, J.C.,: The role of molecular modeling in confined systems: impact and prospects. Phys. Chem. Chem. Phys. (2011). doi:10.1039/c0cp01475c

Hahn, K., Kärger, J.: Deviations from the normal time regime of single-file diffusion. J. Phys. Chem. B **102**, 5766–5771 (1998)

Hahn, K., Kärger, J.: Molecular dynamics simulations of single-file systems. J. Phys. Chem. **100**, 316–326 (1996)

Heink, W., Kärger, J., Pfeifer, H., Vartapetian, R.S., Voloshchuk, A.M.: PFG NMR-study of multicomponent self-diffusion on active carbons. Carbon **31**, 1083–1087 (1993)

Herrera, L.F., Junpirom, S., Do, D.D., Tangsathitkulchai, C.: Computer synthesis of char and its characterization. Carbon **47**, 839–849 (2009)

Hoover, W.G.: Canonical dynamics: equilibrium phase-space distributions. Phys. Rev. A **31**, 1695–1967 (1985)

Jain, S., Pellenq, R., Pikunic, J., Gubbins, K.E.: Molecular modeling of porous carbons using the hybrid reverse Monte Carlo method. Langmuir **22**, 9942–9948 (2006)

Jobic, H.: Neutron scattering methods for the study of zeolites. Curr. Opin. Solid State Mater. Sci. **6**, 415–422 (2002)

Jobic, H., Bee, M., Methivier, A., Combet, J.: Influence of the cation composition on the dynamics of xylenes in x-type zeolites. Microporous Mesoporous Mater. **42**, 135–155 (2001)

Jobic, H., Methivier, A., Ehlers, G.: Different diffusivities of xylene isomers in BaX zeolite measured by the neutron spin echo technique. Microporous Mesoporous Mater. **56**, 27–32 (2002)

Johnson, J., Zollweg, J., Gubbins, K.E.: The Lennard-Jones equation of state revisited. Mol. Phys. **78**, 591–618 (1993)

Kärger, J., Pfeifer, H., Vartapetian, R.S., Voloshchuk, A.M.: Molecular self-diffusion in active carbons. Pure Appl. Chem. **61**, 1875–1880 (1989)

Lastoskie, C., Gubbins, K.E., Quirke, N.: Pore size distribution analysis of microporous carbons: a density functional theory approach. J. Phys. Chem. **97**, 4786–4796 (1993)

Lemmon, E., McLinden, M.O., Friend, D.G.: Thermophysical properties of fluid systems. In: Linstrom, P.J., Mallard, P.J. (eds.) NIST Chemistry WebBook, NIST Standard Reference Database Number 69. National Institute of Standards and Technology, Gaithersburg (2010)

Lísal, M., Brennan, J.K., Smith, W.R.: Chemical reaction equilibrium in nanoporous materials: NO dimerization reaction in carbon slit nanopores. J. Chem. Phys. **124**, 064712 (2006)

Liu, Y.-C., Moore, J.D., Chen, Q., Roussel, T.J., Gubbins, K.E.: Crossover from single-file to Fickian diffusion in carbon nanotubes and nanotube bundles: pure components and mixtures. In: Chmelik, C., Kanellopoulos, N., Kärger, J., Theodoru, D. (eds.) Proceedings of the Diffusion Fundamentals III Conference, pp. 164–180. Leipziger Universitätsverlag, Berlin (2009)

Liu, Y.-C., Moore, J.D., Roussel, T.J., Gubbins, K.E.: Dual diffusion mechanism of argon confined in single-walled carbon nanotube bundles. Phys. Chem. Chem. Phys. **12**, 6632–6640 (2010)

Marks, N.A.: Generalizing the environment-dependent interaction potential for carbon. Phys. Rev. B: Condens. Matter Mat. Phys. **63**, 035401-035407 (2000)

Moore, J.D., Palmer, J.C., Liu, Y.-C., Brennan, J.K., Gubbins, K.E.: Adsorption and diffusion of argon confined in ordered and disordered microporous carbons. Appl. Surf. Sci. **256**, 5131–5136 (2010)

Myers, A., Monson, P.: Adsorption in porous materials at high pressure: theory and experiment. Langmuir **18**, 10261–10273 (2002)

Neimark, A.V., Lin, Y.Z., Ravikovitch, P.I., Thommes, M.: Quenched solid density functional theory and pore size analysis of micro-mesoporous carbons. Carbon **47**, 1617–1628 (2009)

Nguyen, T.X., Bhatia, S.K., Jain, S.K., Gubbins, K.E.: Structure of saccharose-based carbon and transport of confined fluids: hybrid reverse Monte Carlo reconstruction and simulation studies. Mol. Simul. **32**, 567–577 (2006)

Nicholson, D., Parsonage, N.G.: Computer Simulation and the Statistical Mechanics of Adsorption. Academic Press, London (1982)

Norman, G.E., Filinov, V.S.: Investigations of phase transitions by a Monte Carlo method. High Temp. **7**, 216–222 (1969)

Nosé, S.: A unified formulation of the constant temperature molecular dynamics method. J. Chem. Phys. **81**, 511–519 (1984)

Opletal, G., Petersen, T., Malley, B., Snook, I., McCulloch, D., Marks, N., Yarovsky, I.: Hybrid approach for generating realistic amorphous carbon structure using metropolis and reverse Monte Carlo. Mol. Simul. **28**, 927–938 (2002)

Palmer, J.C., Brennan, J.K., Hurley, M.M., Balboa, A., Gubbins, K.E.: Detailed structural models for activated carbons from molecular simulation. Carbon **47**, 2904–2913 (2009)

Palmer, J.C., Llobet, A., Yeon, S.H., Fischer, J.E., Shi, Y., Gogotsi, Y., Gubbins, K.E.: Modeling the structural evolution of carbide-derived carbons using quenched molecular dynamics. Carbon **48**, 1116–1123 (2010)

Pikunic, J., Gubbins, K.E.: Molecular dynamics simulations of simple fluids confined in realistic models of nanoporous carbons. Euro. Phys. J. E **12**, 35–40 (2003)

Plimpton, S.: Fast parallel algorithms for short-range molecular-dynamics. J. Comp. Phys. **117**, 1–19 (1995)

Radosz, M., Hu, X.D., Krutkramelis, K., Shen, Y.Q.: Flue-gas carbon capture on carbonaceous sorbents: toward a low-cost multifunctional carbon filter for "Green" energy producers. Ind. Eng. Chem. Res. **47**, 3783–3794 (2008)

Rouquerol, J., Llewellyn, P., Rouquerol, R.: Is the BET equation applicable to microporous adsorbents. In: Studies in Surface Science and Catalysis, pp. 49–56. Elsevier, Amsterdam (2007)

Santiso, E.E., George, A.M., Sliwinska-Bartkowiak, M., Nardelli, M.B.: Effect of confinement on chemical reactions. Adsorption **11**, 349–354 (2005)

Shi, Y.: A mimetic porous carbon model by quench molecular dynamics simulation. J. Chem. Phys. **128**, 234707–234711 (2008)

Steele, W.: The physical interaction of gases with crystalline solids: I. Gas-solid energies and properties of isolated adsorbed atoms. Surf. Sci. **36**, 317–352 (1973)

Tchouar, N., Benyettou, M., Kadour, F.O.: Thermodynamic, structural and transport properties of Lennard-Jones liquid systems. A molecular dynamics simulations of liquid helium, neon, methane and nitrogen. Int. J. Mol. Sci. **4**, 595–606 (2003)

Thomson, K.T., Gubbins, K.E.: Modeling structural morphology of microporous carbons by reverse Monte Carlo. Langmuir **16**, 5761–5773 (2000)

Tsai, W., Chang, C.: Adsorption of methylene chloride vapor on activated carbons. J. Chem. Tech. Biotech. **61**, 145–151 (1994)

Turner, C.H., Johnson, J.K., Gubbins, K.E.: Effect of confinement on chemical reaction equilibria: The reactions 2NO <-> NO_2 and $N_2 + 3H_2$ <-> $2NH_3$ in carbon micropores. J. Chem. Phys. **114**, 1851–1859 (2001)

van Duin, A., Dasgupta, S., Lorant, F., Goddard, W.: Reaxff: A reactive force field for hydrocarbons. J. Phys. Chem. A **105**, 9396–9409 (2001)

Vuong, T., Monson, P.A.: Monte Carlo simulation studies of heats of adsorption in heterogeneous solids. Langmuir **12**, 5425–5432 (1996)

Wood, W.W.: Monte Carlo calculations for hard disks in isothermal-isobaric ensemble. J. Chem. Phys. **48**, 415–434 (1968)

Wyckoff, R.W.G.: Crystal Structures. Interscience Publishers, New York (1963)

Yushin, G., Nikitin, A., Gogotsi, Y.: Carbide derived carbon. In: Gogotsi, Y. (ed.) Nanomaterials Handbook, pp. 239–282. Taylor & Francis, Boca Raton (2006)